Phase stabilities and spin transitions of $Fe_3(S_{1-x}P_x)$ at high pressure and its implications in meteorites

Tingting Gu[1,2,*], Yingwei Fei[1,2], Xiang Wu[1], and Shan Qin[1]

[1]Key Laboratory of Orogenic Belts and Crustal Evolution, MOE, Peking University & School of Earth and Space Sciences, Peking University, Beijing 100871, China
[2]Geophysical Laboratory, Carnegie Institution of Washington, Washington, D.C., 20015, U.S.A

Abstract

Fe-S-P compounds have been observed in many meteorites and could be the important components in planetary cores. Here we investigated the phase stability of $Fe_3(S,P)$ solid solutions and synthesized high-quality $Fe_3(S_{1-x}P_x)$ high-pressure phases in the multi-anvil press. The physical properties of $Fe_3(S_{0.5}P_{0.5})$ were further studied in the diamond-anvil cell by synchrotron X-ray diffraction and emission spectroscopy. The solubility of S in the $Fe_3(S,P)$ solid solution increases with increasing pressure. The minimum pressure to synthesize the pure Fe_3S and $Fe_3(S_{0.13}P_{0.87})$ is about 21 and 8 GPa, respectively. The observed discontinuity in unit-cell parameters at about 18 GPa is caused by the high-spin to low-spin transition of iron, supported by X-ray emission spectroscopy data. The sulfur solubility in $Fe_3(S,P)$ solid solutions could be an excellent pressure indicator if such solid solutions are found in nature.

Keywords: Iron sulfides, iron phosphides, high pressure, meteorites, spin transition

Introduction

Iron phosphides have been commonly found in iron meteorites, chondrites, and lunar rocks. Early studies reported that phosphorus-bearing Fe-Ni-Cr sulfides, the so-called Q-phase in the Murchison and Murray CM chondrites (Bunch and Chang 1980) and in carbonaceous chondrite clasts from the Jodzie howardite (Bunch et al. 1979; Bunch and Chang 1980), could host xenon (Lewis et al. 1975). They can crystalize to a single phase alloyed with one or several metallic elements, such as schreibersite (Fe_3P) (Clarke and Goldstein 1978) and barringerite [$(Fe,Ni)_2P$] (Buseck 1969), or combined with other non-metallic elements to form much more complex minerals such as perryite [$(Fe,Ni)_8(Si,P)_3$] (Okada et al. 1991). The occurrence of iron phosphides is often found to accompany with iron sulfides and considered to record the thermal dynamic history of the host meteorite. Fe-Ni-S-P phases from the Erevan howardite (Nazarov et al. 2009) and in Lovina meteorite with IIE group (Teplyakova 2011) were generally considered to be a high-temperature product (Nazarov et al. 2009) or a production that undergoes melting when phosphides and sulfides melt locally in metals as a result of impact events with subsequent fast cooling (Teplyakova 2011). Some iron meteorites groups (IIAB, IIIAB, IVA, and IVB) are also believed to have evolved in the Fe-Ni-S-P system (Jones and Drake 1983). In IIIAB type meteorite, schreibersite was found to coexist with troilite (Buchwald 1975; Goldstein et al. 2009), which was interpreted as immiscible Fe-S and Fe-P molten phases (Goldstein et al. 2009). In contrast, in Elga meteorite with IIE type, schreibersite and Fe-Ni-P-S alloy forms rims and

spheres around silicate inclusions, with S and P nearly evenly distributed (Osadchii et al. 1981). Such feature was interpreted as the meteorite experiencing a dynamic pressure process.

Knowledge of phase relations in the Fe-S-P system at high pressure and temperature is essential to interpret the observations and understand the impact history of the meteorites that host the P-bearing iron sulfides. Although the Fe-S-P system shows a large liquid immiscibility field (Raghavan 1988a, 1988b), high-pressure experiments show complete miscibility between Fe-S and Fe-P (Stewart et al. 2007), which could lead to extensive solid solutions such as $Fe(S,P)$, $Fe_2(S,P)$, and $Fe_3(S,P)$. However, the effect of pressure and temperature on the S/P proportion of these solid solutions is largely unknown. For example, Fe_3P with I structure is stable at ambient condition, whereas Fe_3S with the same structure can only form at pressures above 21 GPa (Fei et al. 2000). The solid solutions between Fe_3P and Fe_3S would therefore be sensitive to pressure, and the proportion of sulfur (S) and phosphorus (P) in the solid solution would potentially indicate the *P-T* path of the mineral formation.

Sulfur and phosphorus have also been considered as potential "light elements" that present in planetary cores. Due to the abundance of iron phosphides and iron sulfides in meteorites and the high partition coefficient of sulfur and phosphorus between metal and silicate, they could dissolve into the primary metallic cores of terrestrial planets during early differentiation. Therefore, measurements of the physical properties of the Fe-P-S phases at high pressure will provide constraints on core properties. Previous studies have been focused on iron phosphides, such as $(Fe,Ni)_2P$ (Dera et al. 2008, 2009), FeP (Gu et al. 2011), and Fe_3P(Gu et al. 2014). In this study, we determine the stability field of the high-pressure $Fe_3(S_{1-x}P_x)$ solid solutions in the Fe-S-P system and measure the physical properties of $Fe_3(S_{0.5}P_{0.5})$ up to 40 GPa.

* E-mail: gtt.pku@gmail.com
Present address: Center for High Pressure Science and Technology Advanced Research (HPSTAR), 1690 Cailun Road, Pudong, Shanghai 201203.

METHOD

Sample synthesis

High-pressure synthesis experiments were performed at the Carnegie Institution of Washington's Geophysical Laboratory in an 800-ton multi-anvil apparatus using a 10/5 assembly and a 1500-ton multi-anvil apparatus using an 8/3 assembly (Bertka and Fei 1997). MgO octahedra were used in all experiments. ZrO_2 and $LaCrO_3$ insulators were used in the 10/5 and 8/3 assemblies, respectively (Supplemental Fig. 1[1]). The furnace consisted of a cylindrical resistance rhenium heater. Sample temperatures were measured with a W5%Re/W26%Re thermocouple inserted coaxially. Pressures were determined from the pressure calibration curves for the 10/5 and 8/3 assemblies (Fei et al. 1997; Hirose and Fei 2002). The starting materials were obtained by mixing pure Fe, FeS (99.99% pure, Alfa Aesar product) and Fe_3P (99.5% pure, Alfa Aesar products) powders. Three proportions of these starting materials were prepared, corresponding to the stoichiometric composition of $Fe_3(S_{0.25}P_{0.75})$, $Fe_3(S_{0.5}P_{0.5})$, and $Fe_3(S_{0.75}P_{0.25})$. The starting powders were mixed and grinded, then loaded into a capsule that was made of MgO, Al_2O_3, or olivine single crystal (Supplemental Fig. 2[1]), which were dried in the oven for at least 3 h. Each sample was compressed at room temperature to the target pressure and then heated to the desired temperature at a rate of 50 K/min and stayed at the target pressure and temperature for 24 h. The recovered sample were mounted in epoxy and polished manually in a diamond-based plate with oil as lubricant.

Compositional analysis

Mineral analyses were performed on the JEOL8900L electron probe microanalyzer (EPMA) at the Geophysical Laboratory of the Carnegie Institution of Washington. Operating conditions were 15 kV accelerating voltage, 35 nA beam current, and 1 μm beam diameter for point analysis. Peak counting times ranged from 30 to 60 s. Quantitative analyses were performed using standards such as pyrite FeS_2 and GeP. The precision is better than ±0.1% for the analyzed elements.

X-ray diffraction

The synthesized samples were first measured by X-ray diffraction at ambient conditions using a Rigaku X-ray micro-diffractometer system with an X-ray beam spot of 30 μm and a wavelength of 0.7093 Å (Mo was used as X-ray target). The sample was picked up and mounted on the top of a glass capillary of 100–300 μm diameter. Then the sample was explored for 30–60 min to obtain a high-quality X-ray diffraction pattern.

In situ high-pressure X-ray diffraction experiments were conducted at HPCAT16-BMD beamline (Advanced Photon Source, Argonne National Laboratory), using a symmetric diamond-anvil cell with 300 μm culets. A 130 μm diameter hole was drilled in the pre-indented 40 μm rhenium gasket. Ne was used as pressure medium and calibrant. Intense monochromatic synchrotron X-radiation, with a fixed wavelength of 0.364693 Å, was used for angle-dispersive X-ray diffraction measurements. A collimated X-ray beam (5×12 μm²) was aligned with the center of the sample chamber in the diamond-anvil cell. Diffraction patterns were recorded with a high-resolution Mar (Evanston, Illinois) CCD area detector and then processed with Fit2D software (Hammersley et al. 1996). The detector tilting and the distance between the sample and detector were calibrated against the known lattice parameters of CeO_2.

X-ray emission spectroscopy

The in situ X-ray emission spectroscopy (XES) experiments were conducted at HPCAT 16-ID-D beamline (Advanced Photon Source, Argonne National Laboratory). Details of this method has been reported before (Rueff et al. 1999; Shen et al. 2003). X-ray energy from 7020 to 7080 eV with a step size of 0.25 eV was scanned. Synchrotron X-rays go through monochromator and are focused by horizontal and vertical Kirkpatrick-Baez mirrors. The focused X-rays reached the sample enclosed in a DAC with X-ray transparent Be gasket. The scattered X-ray is then energy-selected by an analyzer and reaches the detector. The spectrometer adopts Rowland circle geometry, of which the sample, the analyzer, and the detector sit on a circle whose diameter corresponds to the analyzer bending radius R. For the K-edge of 3d transition metal, the X-ray energy is usually below 10 keV, helium was used along the X-ray path to minimize signal attenuation by air. Symmetric diamond-anvil cells with 200 and 300 μm culets were used in the experiments. The diameter of the hole in the gasket in which the sample was placed

was about 60–80 μm. A beryllium (Be) gasket with pre-indented 40 μm was used in the XES experiments. Ne was used as the pressure medium and ruby spheres for the pressure calibration.

RESULTS AND DISCUSSION

$Fe_3(S_{1-x}P_x)$ solid solutions

We have conducted 13 experiments to determine the S solubility in the $Fe_3(S_{1-x}P_x)$ solid solutions in the pressure range of 8–21 GPa, using three starting materials with different S/P ratios. Table 1 lists the starting samples, the synthetic conditions, and the run products. Chemical compositions of the synthetic $Fe_3(S_{1-x}P_x)$ solid solutions of the run products were listed on Table 2. At 8 GPa, the synthesized $Fe_3(S_{1-x}P_x)$ contains sulfur with $x = 0.87$, coexisting with $Fe_2(S,P)$ and some residual FeS (Supplemental Fig. 3[1]), using a starting composition containing sulfur with $x = 0.75$. The result indicates the maximum solubility of sulfur in the $Fe_3(S_{1-x}P_x)$ structure is about $x = 0.87$ at 8 GPa.

At 10 GPa, we used starting material with element fraction as $x = 0.75$ and conducted synthesis experiments at temperatures between 1173 and 1273 K, using different capsule materials (MgO, olivine, or Al_2O_3). The quench texture and phase assemblage of the 1273 K run indicate the experimental condition close to the peritectic melting (Fig. 1). Because of slightly higher temperature next to the heater, two melt pockets along both sides were observed (Figs. 1a, 1b, and 1c). At the cold end of the capsule, $Fe_3(S_{1-x}P_x)$ coexists with $Fe_2(S,P)$ (Fig. 1d). Further decreasing the temperature, single $Fe_3(S_{1-x}P_x)$ can be synthesized (Table 1). The observed phase relation is very similar to that in the Fe-FeS system at 21 GPa (Fei et al. 2000). The composition of the synthesized $Fe_3(S_{1-x}P_x)$ is identical to that of the starting composition, indicating 10 GPa is sufficiently high pressure to synthesize the $Fe_3(S_{0.25}P_{0.75})$ solid solution.

Similarly, $Fe_3(S_{0.5}P_{0.5})$ can be obtained at 18 GPa. However, if the same composition was compressed to 16 GPa, the final product contains less sulfur [$Fe_3(S_{0.42}P_{0.58})$], indicating the maximum solubility of sulfur in the $Fe_3(S_{1-x}P_x)$ structure is about 0.42 at 16 GPa. At 21 GPa, we also synthesized homogenous $Fe_3(S_{0.75}P_{0.25})$ solid solution as confirmed by chemical composition map (Fig. 2). It is clear that the sulfur solubility in the $Fe_3(S_{1-x}P_x)$ structure increases with pressure. Figure 3 shows the composition of the

TABLE 1. Synthetic conditions of each runs and the final products observed under SEM

Run no.	P (GPa)	T (K)	Capsule materials	Run products
Starting compositions: Fe, FeS, Fe_3P [2:1:3, $Fe_3(S_{0.25}P_{0.75})$][a]				
S8	8	1173	Olivine	$Fe_3(S,P)$, FeS, $Fe_2(S,P)$
S1	10	1273	MgO	$Fe_3(S,P)$, $Fe_2(S,P)$, melt
S2	10	1200	MgO	$Fe_3(S,P)$, $Fe_2(S,P)$
S3	10	1175	MgO	$Fe_3(S,P)$
S4	10	1196	Olivine	$Fe_3(S,P)$
S5	10	1200	Al_2O_3	$Fe_3(S,P)$
S9	10	1173	Olivine	$Fe_3(S,P)$
Starting compositions: Fe, FeS, Fe_3P [2:2:1, $Fe_3(S_{0.5}P_{0.5})$]				
bs1	16	1173	MgO	$Fe_3(S,P)$, $Fe_2(S,P)$
bs3	16	1173	MgO	$Fe_3(S,P)$, $Fe_2(S,P)$
S-2-1	18	1173	Olivine	$Fe_3(S,P)$, FeS, $Fe_2(S,P)$
S-2-4	18	1173	Olivine	$Fe_3(S,P)$
Starting compositions: Fe, FeS, Fe_3P [2:3:1, $Fe_3(S_{0.75}P_{0.25})$]				
S-3-1	21	1140	Al_2O_3	$Fe_3(S,P)$
S-3-2	21	1173	Olivine	$Fe_3(S,P)$

[a] Starting material was obtained by mixing pure Fe, FeS (99.99% pure, Alfa Aesar product), and Fe_3P (99.5% pure, Alfa Aesar products) powders. Three proportions of these starting materials were prepared, corresponding to the stoichiometric composition of $Fe_3(S_{0.25}P_{0.75})$, $Fe_3(S_{0.5}P_{0.5})$, and $Fe_3(S_{0.75}P_{0.25})$.
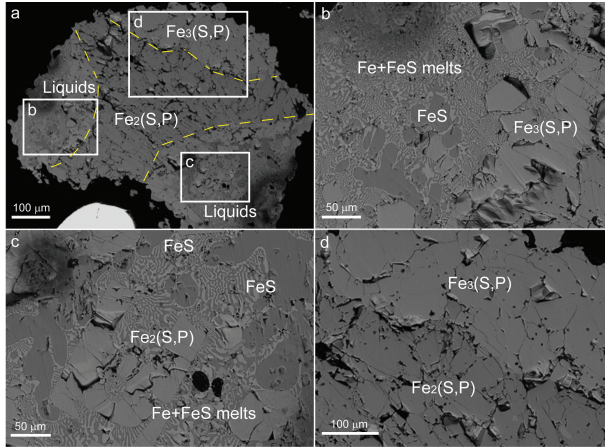
FIGURE 1. Backscatter electron images of sample quenched from 10 GPa, 1000 °C in a MgO capsule, showing an equilibrium feature of liquids and solid solutions. (**a**) An image of the whole sample. Dashed lines were marked along the phase boundaries. The details of the marked areas are shown in the rest images (**b–c**). (**b**) Phase boundary where Fe and FeS melts coexist with $Fe_2(S,P)$ solid solutions. (**c**) The liquids, where Fe and FeS surround over $Fe_2(S,P)$ grains. (**d**) Phase boundary between $Fe_2(S,P)$ and $Fe_3(S,P)$ solid solutions. (Color online.)

FIGURE 3. The maximum solubility of S in $Fe_3(S_{1-x}P_x)$ solid solution at about 1173–1200 K as a function of pressure. The circles, squares, and solid diamonds represent data obtained with MgO, Al_2O_3, and olivine capsules, respectively. The open diamonds indicate the spin transition pressures (Shen et al. 2003; Lin et al. 2004). Dotted arrows indicate the S/P ratios of the starting compositions. The area between the dashed lines illustrates the uncertainty of the spin transition. *Note:* Dashed and solid lines are guides for eyes. (Color online.)

synthesized $Fe_3(S_{1-x}P_x)$ solid solution as a function of pressure. The result is consistent with previous study on the formation of Fe₃S at 21 GPa and subsolidus temperatures (Fei et al. 2000).

Bulk modulus of $Fe_3(S_{1-x}P_x)$

The high-pressure $Fe_3(S_{1-x}P_x)$ solid solutions are quenchable. We performed X-ray diffraction measurements at ambient conditions on samples that are homogenous. From their XRD patterns, all peaks can be indexed as $I\overline{4}$ structure (isostructural to Fe₃P) (Supplemental Fig. 4[1]). Rietveld refinements were applied for each pattern by GSAS software and their volumes were obtained and plotted as a function of composition in Figure 4. The values of the volumes and unit-cell parameters show a roughly linear relationship with the amount of sulfur in the solid solution.

To investigate the structure stability and compression behavior, we performed in situ high-pressure experiments on $Fe_3(S_{0.5}P_{0.5})$ by diamond-anvil cell technique. The in situ XRD patterns were collected up to 30 GPa at room temperature.

Supplemental Figure 5[1] shows several representative patterns. All peaks can be indexed as I Fe₃P structure and cubic Ne (pressure-transmitting medium). At each point, the pressure was measured from the Raman shifts of diamond culet at the center and the edge (Akahama and Kawamura 2004). The average pressure was used and pressure gradient was calculated (Fig. 5); meanwhile, pressures obtained by diffraction of solid neon (Fei et al. 2007) above 7 GPa were listed in comparison in Supplemental Table 2[1]. Unit-cell parameters of $Fe_3(S_{0.5}P_{0.5})$ were refined by a model based on Le Bail whole profile fitting implemented in the GSAS software (Toby 2001; Larson and Von Dreele 2004). At each pressure, the volume and c/a ratio were plotted in Figure 4, compared with results of Fe₃P (Scott et al. 2007; Gu et al. 2014) and Fe₃S (Fei et al. 2000). Data of $Fe_3(S_{0.5}P_{0.5})$ below 20 GPa were fitted by second-order Birch-Murnaghan equation of state, with V_0 fixed at 373.016 Å³, yielding $B_0 = 158(1)$ GPa, $B'_0 = 4$, which is between the B_0 value of Fe₃S and Fe₃P (Supplemental Table 1[1]). A discontinuity in the c/a ratio was observed around
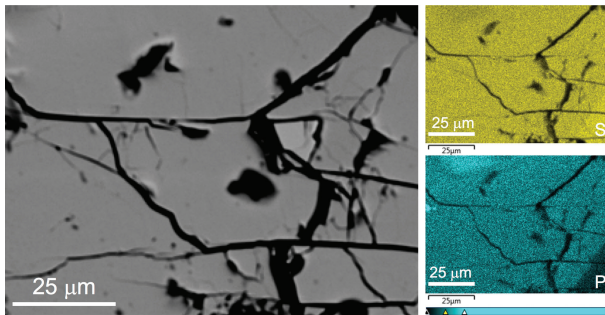

FIGURE 2. Backscatter electron image of the sample quenched from 21 GPa, 900 °C in an olivine capsule. The chemical maps of S and P show homogeneous distribution of P and S in the sample. (Color online.)
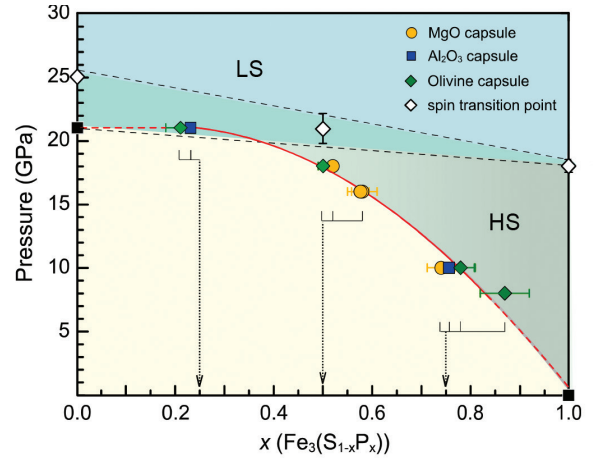
TABLE 2. Chemical compositions of the synthetic $Fe_3(S_{1-x}P_x)$ solid solutions (wt%)[a]

Run no.	Fe	P	S	Mg	Al	Si	O	Total	x
S1	84.1(3)	12.1(6)	3.3(5)	–	–	–	–	99.5	0.79(4)
S1[b]	77.3(4)	13.5(3)	8.3(4)	–	–	–	–	99.1	0.63(3)
S3	81.4(3)	11.5(4)	4.1(5)	0.94(4)	0.5(2)	–	1.6(1)	100.7	0.74(3)
bs1	83.7(5)	8.9(3)	6.7(5)	0.7(3)	–	–	–	100.0	0.58(2)
bs3	83.3(3)	8.9(5)	6.5(5)	0.5(2)	–	–	–	99.2	0.58(3)
S4	83.7(5)	12.4(5)	3.5(4)	0.1(2)	–	0.1(2)	–	99.9	0.78(3)
S9	83.9(2)	12.5(5)	3.6(5)	–	–	–	–	100.0	0.78(3)
S8	83.7(1)	14.2(8)	2.1(9)	–	–	–	–	100.0	0.87(5)
S-2-1	84.1(3)	8.0(5)	7.5(6)	–	–	–	–	100.9	0.52(3)
S-2-4	84.3(2)	7.6(3)	7.8(3)	–	–	–	–	99.7	0.50(1)
S-3-2	83.4(6)	3.2(4)	12.3(4)	0.3(1)	–	0.1(1)	–	99.4	0.21(3)
S5	84.3(9)	12.5(6)	3.4(8)	–	0.5(8)	–	–	100.7	0.76(1)
S-3-1	83.1(7)	3.5(2)	11.9(1)	–	0.5(1)	–	–	99.1	0.23(1)

[a] Numbers in parentheses represent analyses uncertainties.
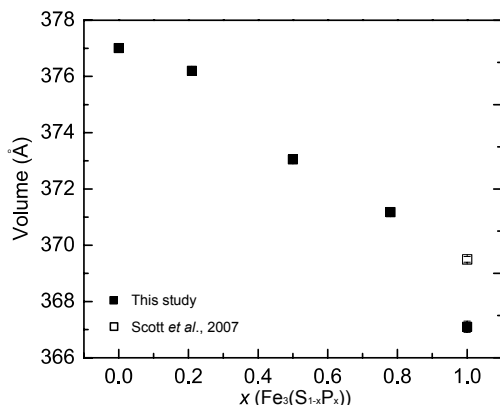[b] Chemical composition of $Fe_2(S_{1-x}P_x)$ in sample S1.

FIGURE 4. Relationship between volume and composition of the synthesized $Fe_3(S_{1-x}P_x)$ solid solutions at ambient conditions.
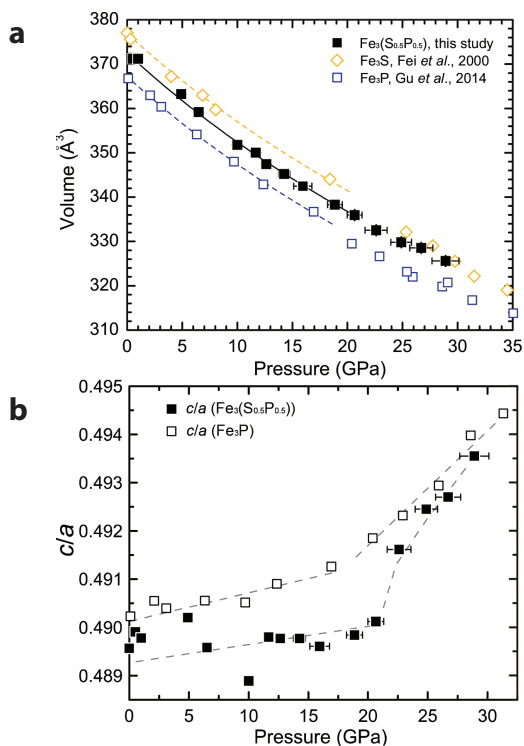

FIGURE 5. Volumes and unit-cell parameters of $Fe_3(S_{0.5}P_{0.5})$ as a function of pressure. (**a**) Volumes of $Fe_3(S_{0.5}P_{0.5})$ as a function of pressure, fitted by B-M equation of state. Data of Fe_3P and Fe_3S were also plotted for comparison; B' was fixed at 4. (**b**) Changes of the c/a ratios of $Fe_3(S_{0.5}P_{0.5})$ and Fe_3P as a function of pressure. Dash lines are guide for eyes. Note the discontinuous change of c/a ratio of the two samples. (Color online.)

21 GPa (Fig. 4), which reflects a spin crossover, also observed in Fe_3P (Gu et al. 2014) and Fe_3S (Chen et al. 2007).

X-ray emission spectroscopy and the spin transition

To confirm the spin transition indicated by the observed discontinuity in volume and cell parameters, X-ray emission spectroscopy was performed on Fe_3P and $Fe_3(S_{0.5}P_{0.5})$ up to 64
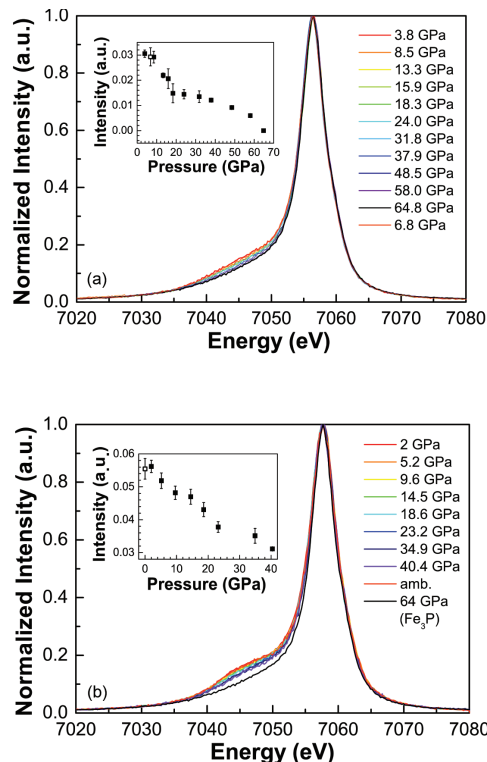

FIGURE 6. X-ray emission spectroscopy of Fe_3P (**a**) and $Fe_3(S_{0.5}P_{0.5})$ (**b**) at different pressures. Insets: relative intensity of $K\beta'$ peaks as a function of pressure. (Color online.)

and 40 GPa, respectively. Figure 6a shows the Fe$K\beta$ XES of Fe_3P between ambient pressure and 64 GPa. All spectra are normalized to transmitted intensity, and also shifted to set the peak of the Fe $K\beta_{1,3}$ main emission line to 7058 eV. The width of the $K\beta_{1,3}$ peak significantly narrows down at higher pressures. A well-defined satellite located at 7045.5 eV and denoted to $K\beta'$, presents up to 64 GPa, with its intensity gradually diminishing as pressure increases. The observed changes are reversible as decompressed to ambient pressure.

The $K\beta$ spectra of $Fe_3(S_{0.5}P_{0.5})$ were normalized to unit area and plotted in Figure 6b. The relative intensity of $K\beta'$ satellite at 7045.5 eV was determined by subtracting each spectrum from that one of Fe_3P at 64 GPa, which is shown as a reference in the figure. The relative intensities for Fe_3P and $Fe_3(S_{0.5}P_{0.5})$ as a function of pressure were shown in the insets of Figure 6. In the case of Fe_3P, the slope of the satellite intensity shows an abrupt change at ~18.3 GPa, while a subtle non-linear decrease of the satellite intensity is observed at ~40 GPa. The X-ray emission spectroscopic data are consistent with the observed discontinuous changes in lattice parameter of Fe_3P at 18 and 40 GPa as reported by (Gu et al. 2014). In comparison, the discontinuous decrease of $K\beta'$ satellite intensity of $Fe_3(S_{0.5}P_{0.5})$ is observed at a slightly higher pressure (~23 GPa).

DISCUSSIONS AND IMPLICATIONS

Theoretical studies (de Groot et al. 1995; Peng et al. 1994) indicate that the $K\beta$ emission is dominated by final state interac-

tion between the 3p core hole and the electrons of the partially filled 3d shell, which will result in splitting of the $K\beta$ spectrum into HS and LS final states. At HS state, the $3p\downarrow3d\uparrow$ final state will further split into two components, one main peak with a shoulder at slightly lower energy than the main emission line ($3p\uparrow3d\uparrow$). At LS state, a $3p\uparrow3d\uparrow$ final state will result in a single peak. For Fe^{2+}, the electrons occupy the orbitals according to Hund's rule. The final electronic configuration of the LS state becomes $t_{2g\uparrow}^3 t_{2g\downarrow}^3$ with a total 3d magnetic moment of zero, and the $K\beta'$ line is expected to disappear. On the other hand, the electronic configuration for Fe^{3+} is $t_{2g\uparrow}^3 t_{2g\downarrow}^2$, thus the magnitude of magnetic moment would depend on the nature of the ligand field and 3d band structure, and a finite moment would be expected in the LS state. In the structure of Fe_3P, iron atoms present at three different positions, thus their valence state of each iron would be more complex. According to Mössbauer spectroscopy of Fe_3P, there are six sextets of Fe_3P, and the isomer shift of them is between 0.27–0.40 mm/s (Lisher et al. 1974), which falls in the range of Fe^{3+}. It is likely that the observed discontinuity of $K\beta'$ satellite intensity at ~18 GPa is associated with the HS to LS transition of Fe^{3+}.

At higher pressure, the magnetic moment of Fe_3P begins to collapse. Theoretical study showed that Fe_3P loses magnetic moments at about 60 GPa (Gu et al. 2014). The intensity decrease of $K\beta'$ satellite at ~40 GPa is related to the magnetic collapse of Fe. In the case of $Fe_3(S_{0.5}P_{0.5})$, the HS to LS transition pressure is slightly higher than that of Fe_3P, which would be attributed to a different 3d band structure affected by stronger p-d hybridization of Fe and S.

According to our multi-anvil experiments as well as in situ high-pressure spectroscopy studies, we constructed a diagram indicating the maximum sulfur concentration in $Fe_3(S_{1-x}P_x)$ solid solution at 900 °C as a function of pressure together with the spin transition boundaries (Fig. 3). The $Fe_3(S_{1-x}P_x)$ solid solutions synthesized at the sulfur contents below $x = 0.5$ are at high-spin state. The maximum solubility of sulfur in $Fe_3(S_{1-x}P_x)$ increases almost linearly with pressure, up to $x = 0.5$ at 18 GPa. The end-member Fe_3S forms at 21 GPa as reported by Fei et al. (1997) and there is very small pressure dependence to form $Fe_3(S_{1-x}P_x)$ at the sulfur contents above $x = 0.5$. The dramatic change of the pressure effect on the sulfur solubility in the $Fe_3(S_{1-x}P_x)$ structure at around 18 GPa might be related to the spin transition that occurs at that pressure. Easy incorporation of sulfur into the $Fe_3(S_{1-x}P_x)$ structure could result from the reduction of the atomic size of iron at low-spin state. The atomic size ratio of S/Fe would be more close to that of P/Fe after the spin transition because the atomic size of sulfur is ~3% smaller than that of phosphorus. Such crystallographic configuration tends to facilitate the incorporation of sulfur atoms into $Fe_3(S_{1-x}P_x)$ solid solutions.

Fe_3S can only be synthesized at pressures above 21 GPa, but it is quenchable in the same structure as Fe_3P. If Fe_3S were ever found in meteorites, it would be an unambiguous high-pressure indicator with a minimum shock pressure of 21 GPa. The $Fe_3(S_{1-x}P_x)$ solid solutions, on the other hand, is an effective pressure scale that can be used to pinpoint the formation pressure because the maximum sulfur solubility in schreibersite is pressure sensitive. It would potentially be an indicator of the thermodynamic path of its host meteorites if such solid solution were found.

Because $Fe_3(S_{1-x}P_x)$ solid solutions have low melting temperature, it would be challenging to find the solid solutions in meteorites that undergo complex dynamic pressure conditions. Byproducts such as $Fe_2(S,P)$ solid solutions with quenched melt texture could indicate that the meteorite experienced a high temperature above the eutectic point of $Fe_3(S,P)$. Although schreibersite with significant amount of sulfur has not been founded yet (Nazarov et al. 2009), under proper shock pressure conditions, fine grains of $Fe_3(S,P)$ solid solutions might preserve. The discovery of a first natural $Fe_3(S,P)$ solid solution has to rely on a systematic search through shocked meteorites with sulfur-bearing schreibersite.

REFERENCES CITED

Akahama, Y., and Kawamura, H. (2004) High-pressure Raman spectroscopy of diamond anvils to 250 GPa: Method for pressure determination in the multimegabar pressure range. Journal of Applied Physics, 96, 3748–3751.

Bertka, C.M., and Fei, Y. (1997) Mineralogy of martian interior up to core–mantle boundary pressures. Journal of Geophysical Research, 102, 5251–5264.

Buchwald, V.F. (1975) Handbook of Iron Meteorites. Their History, Distribution, Composition and Structure 1. University California Press, Berkeley.

Bunch, T.E., and Chang, S. (1980) Carbonaceous chondrites—II. Carbonaceous chondrite phyllosilicates and light element geochemistry as indicators of parent body processes and surface conditions. Geochimica et Cosmochimica Acta, 44, 1543–1577.

Bunch, T.E., Chang, S., Frick, U., Neil, J., and Moreland, G. (1979) Carbonaceous chondrites–-I. Characterization and significance of carbonaceous chondrite (CM) xenoliths in the Jodzie howardite. Geochimica et Cosmochimica Acta, 43, 1727–1742.

Buseck, P.R. (1969) Phosphide from metorites: barringerite, a new iron-nickel mineral. Science, 165, 169–171.

Chen, B., Gao, L., Funakoshi, K.-I., and Li, J. (2007) Thermal expansion of iron-rich alloys and implications for the Earth's core. Proceedings of the National Academy of Sciences, 104, 9162–9167.

Clarke, R.S., and Goldstein, J. (1978) Schreibersite growth and its influence on the metallography of coarse-structured iron meteorites, 83 p. Smithsonian Contributions to the Earth Sciences, no. 21. Smithsonian Institution Press, Washington, D.C.

de Groot, F.M.F., Pizzini, S., Fontaine, A., Hämäläinen, K., Kao, C.C., and Hastings, J.B. (1995) Local-spin-selective X-ray absorption and X-ray magnetic circular dichroism of MnP. Physical Review B, 51, 1045–1052.

Dera, P., Lavina, B., Borkowski, L.A., Prakapenka, V.B., Sutton, S.R., Rivers, M.L., Downs, R.T., Boctor, N.Z., and Prewitt, C.T. (2008) High-pressure polymorphism of Fe₂P and its implications for meteorites and Earth's core. Geophysical Research Letters, 35, L10301.

——— (2009) Structure and behavior of the barringerite Ni end-member, Ni₂P, at deep Earth conditions and implications for natural Fe-Ni phosphides in planetary cores. Journal of Geophysical Research, 114, B03201.

Fei, Y.W., Bertka, C.M., and Finger, L.W. (1997) High-pressure iron-sulfur compound, Fe₃S₂, and melting relations in the Fe-FeS system. Science, 275, 1621–1623.

Fei, Y.W., Li, J., Bertka, C.M., and Prewitt, C.T. (2000) Structure type and bulk modulus of Fe₃S, a new iron-sulfur compound. American Mineralogist, 85, 1830–1833.

Fei, Y., Ricolleau, A., Frank, M., Mibe, K., Shen, G., and Prakapenka, V. (2007) Toward an internally consistent pressure scale. Proceedings of the National Academy of Sciences, 104, 9182–9186.

Goldstein, J.I., Scott, E.R.D., and Chabot, N.L. (2009) Iron meteorites: Crystallization, thermal history, parent bodies, and origin. Chemie der Erde–Geochemistry, 69, 293–325.

Gu, T., Wu, X., Qin, S., and Dubrovinsky, L. (2011) In situ high-pressure study of FeP: Implications for planetary cores. Physics of the Earth and Planetary

Interiors, 184, 154–159.

Gu, T., Fei, Y., Wu, X., and Qin, S. (2014) High-pressure behavior of Fe_3P and the role of phosphorus in planetary cores. Earth and Planetary Science Letters, 390, 296–303.

Hammersley, A.P., Svensson, S.O., Hanfland, M., Fitch, A.N., and Häusermann, D. (1996) Two-dimensional detector software: From real detector to idealised image or two-theta scan. High Pressure Research, 14, 235–248.

Hirose, K., and Fei, Y. (2002) Subsolidus and melting phase relations of basaltic composition in the uppermostlower mantle. Geochimica et Cosmochimica Acta, 66, 2099–2108.

Jones, J.H., and Drake, M.J. (1983) Experimental investigations of trace element fractionation in iron meteorites, II: The influence of sulfur. Geochimica et Cosmochimica Acta, 47, 1199–1209.

Larson, A.C., and Von Dreele, R.B. (2004) General Structure Analysis System (GSAS). Los Alamos National Laboratory Report LAUR 86-748.

Lewis, R.S., Srinivasan, B., and Anders, E. (1975) Host phase of a strange xenon component in Allende. Science, 190, 1251–1262.

Lin, J.-F., Fei, Y., Sturhahn, W., Zhao, J., Mao, H.-K., and Hemley, R.J. (2004) Magnetic transition and sound velocities of Fe_3S at high pressure: implications for Earth and planetary cores. Earth and Planetary Science Letters, 226, 33–40.

Lisher, E.J., Wilkinson, C., Ericsson, T., Haggstrom, L., Lundgren, L., and Wappling, R. (1974) Studies of the magnetic structure of Fe_3P. Journal of Physics C: Solid State Physics, 1344–1352.

Nazarov, M.A., Kurat, G., Brandstaetter, F., Ntaflos, T., Chaussidon, M., and Hoppe, P. (2009) Phosphorus-bearing sulfides and their associations in CM chondrites. Petrology, 17, 101–123.

Okada, A., Kobayashi, K., Ito, T., and Sakurai, T. (1991) Structure of synthetic perryite, $(Ni,Fe)_8(Si,P)_3$. Acta Crystallographica C, 47, 1358–1361.

Osadchii, E.G., Novikov, G.V., and Baryshnikova, G.V. (1981) The Elga meteorite: Silicate inclusions and shock metamorphism. Lunar and Planetary Science Conference, 12, 1049–1068.

Peng, G., de Groot, F.M.F., Hämäläinen, K., Moore, J.A., Wang, X., Grush, M.M., Hastings, J.B., Siddons, D.P., and Armstrong, W.H. (1994) High-resolution manganese X-ray fluorescence spectroscopy. Oxidation-state and spin-state sensitivity. Journal of the American Chemical Society, 116, 2914–2920.

Raghavan, V. (1988a) Phase Diagrams of Ternary Iron Alloys. Pt. 3. Ternary Systems Containing Iron and Phosphorus, 1 p. Indian Institute of Metals, Calcutta.

——— (1988b) Phase Diagrams of Ternary Iron Alloys: Ternary systems containing iron and sulphur, 1 p. Indian Institute of Metals, Calcutta.

Rueff, J.P., Kao, C.C., Struzhkin, V.V., Badro, J., Shu, J., Hemley, R.J., and Mao, H.-K. (1999) Pressure-induced high-spin to low-spin transition in FeS evidenced by X-ray emission spectroscopy. Physical Review Letters, 82, 3284–3287.

Scott, H.P., Huggins, S., Frank, M.R., Maglio, S.J., Martin, C.D., Meng, Y., Santillán, J., and Williams, Q. (2007) Equation of state and high-pressure stability of Fe_3P-schreibersite: Implications for phosphorus storage in planetary cores. Geophysical Research Letters, 34, L06302.

Shen, G., Lin, J.-F., Fei, Y., Mao, H.-K., Hu, M., and Chow, P. (2003) Magnetic and structural transition in Fe_3S at high pressures. Eos, Transactions American Geophysical Union, 84, F1548–F1549.

Stewart, A.J., Schmidt, M.W., Westrenen, W.V., and Liebske, C. (2007) Mars: A new core-crystallization regime. Science, 316, 1323–1325.

Teplyakova, S.N. (2011) Evolution of molten material in iron cores of small planets. Solar System Research, 45, 515–522.

Toby, B.H. (2001) EXPGUI, a graphical user interface for GSAS. Journal of Applied Crystallography, 34, 210–213.